Bioactive Materials 6 (2021) 3692–3704

Contents lists available at ScienceDirect

Bioactive Materials

journal homepage: www.sciencedirect.com/journal/bioactive-materials

Modulating degradation of sodium alginate/bioglass hydrogel for improving tissue infiltration and promoting wound healing

Xin Zhang [a], Ying Li [a], Zhijie Ma [a], Dan He [a], Haiyan Li [a,b,*]

[a] School of Biomedical Engineering, Shanghai Jiao Tong University, 1954 Huashan Road, Shanghai, 200030, China
[b] Chemical and Environmental Engineering, School of Engineering, RMIT University, 124 La Trobe St, Melbourne, VIC, 3000, Australia

ARTICLE INFO

Keywords:
Sodium alginate
Bioglass
Hydrogels degradation
Tissue infiltration
Wound healing

ABSTRACT

More and more studies have recognized that the nanosized pores of hydrogels are too small for cells to normally grow and newly formed tissue to infiltrate, which impedes tissue regeneration. Recently, hydrogels with macropores and/or controlled degradation attract more and more attention for solving this problem. Sodium alginate/Bioglass (SA/BG) hydrogel, which has been reported to be an injectable and bioactive hydrogel, is also limited to be used as tissue engineering scaffolds due to its nanosized pores. Therefore, in this study, degradation of SA/BG hydrogel was modulated by grafting deferoxamine (DFO) to SA. The functionalized grafted DFO-SA (G-DFO-SA) was used to form G-DFO-SA/BG injectable hydrogel. In vitro degradation experiments proved that, compared to SA/BG hydrogel, G-DFO-SA/BG hydrogel had a faster mass loss and structural disintegration. When the hydrogels were implanted subcutaneously, G-DFO-SA/BG hydrogel possessed a faster degradation and better tissue infiltration as compared to SA/BG hydrogel. In addition, in a rat full-thickness skin defect model, wound healing studies showed that, G-DFO-SA/BG hydrogel significantly accelerated wound healing process by inducing more blood vessels formation. Therefore, G-DFO-SA/BG hydrogel can promote tissue infiltration and stimulate angiogenesis formation, which suggesting a promising application potential in tissue regeneration.

1. Introduction

Hydrogels are 3D polymer network composed of a hydrophilic skeleton, which own good water retention ability [1]. Due to the structure similarity between hydrogels and extracellular matrix of tissues, hydrogels have received intensive attention in tissue engineering [2]. Compared with other solid scaffolds (ceramics, metal implant), hydrogels have many advantages, such as adjustable physical and chemical properties, possible injectable for non-invasive implantation, friendly to encapsulated bioactive molecules, and helpful for wound healing with the moist environment [3–6]. Thus, hydrogels have played a key role in many drug delivery systems and tissue regeneration [7,8]. However, nanosized pores of hydrogels have become an intrinsic deficiency in tissue regeneration since they are too small for cells to normally grow and newly formed tissue to infiltrate, and as a result, tissue regeneration is usually impeded [9]. Macroporous hydrogels and degradable hydrogels are common solutions for this concern. For example, Griffin et al. fabricated an injectable microporous gel scaffold for accelerating wound healing. The microporous gel scaffold was assembled by annealed building blocks and proved to effectively facilitate cell migration into the scaffold [10]. Speeding up the degradation of hydrogels is another way to make hydrogels suitable for tissue infiltration. An enzymatically degradable hydrogel was proved to be able to accelerate cell infiltration when it was implanted in subcutaneous by incorporating minimal elastase substrate peptide into the branched poly (ethylene glycol) macromonomer structure [11]. A typical method for constructing macroporous hydrogels is the assembly of microgels [12]. Microfluidic emulsion and lithography are the most used technologies for microgels production [10,13]. Microfluidic emulsion method requires that hydrogel precursor solutions must be relatively low viscose and can be quickly crosslinked during collection. These specific requirements have been a great limitation for the further promotion of microfluidic emulsion method. Besides, the low production rate of microgels is an intrinsic deficiency for lithography technology [12]. Therefore, the difficulty of obtaining microgels limits the widespread use of macroporous gels. Proposing an easy-to-implement strategy to

Peer review under responsibility of KeAi Communications Co., Ltd.
* Corresponding author. School of Biomedical Engineering, Med-X Research Institute Shanghai Jiao Tong University, 1954 Huashan Road, Shanghai, 200030, China.
E-mail addresses: haiyan.li@sjtu.edu.cn, haiyan.li4@rmit.edu.au (H. Li).

https://doi.org/10.1016/j.bioactmat.2021.03.038
Received 24 December 2020; Received in revised form 3 March 2021; Accepted 26 March 2021

accelerate hydrogel degradation is necessary and urgent for this concern.

Among the numerous hydrogel skeleton materials, sodium alginate (SA) has received extensive attention because of its good biocompatibility and wide range of source. SA hydrogels can be formed by covalent crosslinking and divalent cation crosslinking [14]. Bioglass (BG) is a kind of man-made oxide-based biomaterials with multiple bioactivities and BG has been widely used in hard tissue and soft tissue regeneration [15,16]. In our previous study, an injectable bioactive SA/Bioglass (SA/BG) hydrogel has been designed. This injectable hydrogel was achieved by simply repeatedly pipetting SA precursor and BG powders in a t-branch pipe with the presence of Gluconic acid δ-lactone [17]. Ions released from BG can simultaneously endow the hydrogel with multiple biological activities, such as stimulatory abilities for angiogenesis and osteogenic differentiation [18,19]. In addition, we have proved that SA/BG hydrogel had excellent therapeutic effects in wound healing, osteochondral regeneration, and post-infarct myocardial regeneration [17,20,21]. Although SA/BG hydrogel has the above-mentioned advantages on tissue regeneration, there are still obstacles for the hydrogel to be used clinically and the most critical problem is that the nanosized pores in the hydrogel are too small for cells and tissue infiltration. For example, in an irregular bone repair model, we found that SA/BG hydrogel remained a lot at the implantation site 12 weeks post-surgery, and almost no cells infiltrated into the interior of the hydrogel [22]. Unfortunately, this is a general problem of all SA-based hydrogels. Due to the lack of homologous enzymes in vivo and high crosslinking density, implanted SA-based hydrogels are usually difficult to degrade and tend to maintain the original nanosized network, which impedes the infiltration of cells and newly formed tissue [23].

Many studies have been carried out to accelerate the degradation rate of SA hydrogels in vivo. Oxidizing SA can accelerate the degradation of hydrogel by promoting its hydrolysis. However, oxidized SA introduces aldehyde groups, which may change the biocompatibility of SA [24]. Recently, Lueckgen et al. reported an enzymatically degradable SA hydrogel. This hydrogel was crosslinked by a matrix metalloproteinase sensitive peptide crosslinker which could be specifically cleaved by cells. Thereby, large pores were created after the crosslinker was cleaved by cells and tissue could infiltrate into the hydrogel. However, quantitative analysis revealed that there was only a slight improvement in tissue infiltration. Specifically, tissue infiltration was 16.3% in degradable hydrogel compared with 12.7% in control [25]. Under the premise of good biocompatibility, SA hydrogels with proper degradation rate to facilitate tissue infiltration need to be proposed. The degradation rate of SA hydrogels largely depends on the crosslinking density. Basically, the lower the density of crosslinking, the faster the degradation [26]. Since ionically crosslinked SA hydrogels rely on the carboxyl group on the G block, modulating the number of carboxyl groups on the G block may be a feasible way to adjust the degradation of SA hydrogels.

Deferoxamine (DFO) is a commercial medicine for treating iron poisoning and there is an amine group on the molecule structure of DFO. Considering the carboxyl groups on the SA, it is theoretically feasible to graft DFO onto the SA molecules through an amide reaction and this graft reaction would occupy part of carboxyl groups on the G block. After these reactions, it can be hypothesized that the crosslinking density of SA-based hydrogels can be decreased and thus the degradation rate of the SA hydrogels can be accelerated. In addition, recent research showed that DFO could promote neovascularization by up-regulating the expression of hypoxia-inducible factor-1α (Hif-1α) and vascular endothelial growth factor (VEGF) in cells [27]. Considering the advantages of DFO in promoting angiogenesis, some studies have tried to combine DFO with scaffolds to accelerate wound healing [28,29]. However, DFO was usually physically encapsulated or absorbed within these scaffolds, which resulted in a burst release of DFO in the first 24 h and fully release of DFO within 36 h after the scaffolds were implanted in vivo. Lots of studies have proved that controlled release could be achieved by chemically conjugating DFO with the material of scaffolds [30]. Therefore, it can be assumed that grafting DFO onto the SA molecular can not only modulate the degradation of SA-based hydrogels but also control the release behavior of DFO from the hydrogels.

Thus, in this article, DFO was grafted to SA and this functionalized SA was used to prepare an injectable grafted DFO-SA/BG (G-DFO-SA/BG) hydrogel. We hypothesize that the grafting of DFO can reduce the crosslinking density of the SA/BG hydrogel by consuming part of the carboxyl groups on the SA. Thereby, G-DFO-SA/BG hydrogel with a fast degradation rate can be achieved without changing the biocompatibility of the SA/BG hydrogel. To prove our hypothesis, mass loss, mechanical properties, microstructure, and release behaviors of calcium ions of the hydrogels were investigated to characterize the degradation behaviors of the G-DFO-SA/BG and SA/BG hydrogels in vitro. Then, the hydrogels were implanted subcutaneously to observe the tissue infiltration and degradation behavior of hydrogels in vivo. Finally, the hydrogels were applied to a full-thickness skin excision model in rats to verify the vascularization ability of hydrogels in order to prove the potential applications of the G-DFO-SA/BG hydrogel in wound healing.

2. Materials and methods

2.1. Materials

Sodium alginate (medium viscosity) and Gluconic acid δ-lactone (GDL, > 99.0%) were purchased from Sigma-Aldrich (Santa Clara, USA). Bioglass (BG) (45S glass) powders with an average diameter of 20 μm (90% < 34.86 μm) were purchased from Kunshan Chinese Technology New Materials Co., Ltd (Kunshan, China). 2-(N-morpholino) ethanesulfonic acid (MES), N-(3-Dimethylaminopropyl)-N′-ethylcarbodiimide hydrochloride (EDC) and N-Hydroxysuccinimide (NHS) were obtained from Aladdin Reagent Company (Beijing, China). Deferoxamine mesylate salt (DFO, >92%) was obtained from Yuanye Biotechnology Co., Ltd (Shanghai, China).

2.2. Cell culture

Human umbilical vein endothelial cells (HUVECs) and human dermal fibroblasts (HDFs) were used for cell experiments. HUVECs were used to evaluate the biocompatibility, cell migration, and angiogenesis while HDF cells were used for biocompatibility evaluation and cell migration. HUVECs and HDFs were purchased from Zhong Qiao Xin Zhou Biotechnology Co,Ltd. (Shanghai, China). HUVECs were cultured with endothelial cell medium (ECM, Sciencell, USA). When the HUVECs were cultured to passage 3–5, they were used for cell experiments. HDF cells were cultured with dulbecco's modified eagle medium (DMEM, Gibco, USA) containing 10% FBS and 1% P/S. The HDF cells were used at passaged 7–10 for experiments.

2.3. Synthesis and characterization of the grafted DFO-SA

DFO grafted SA was synthesized by carbodiimide chemistry. Briefly, 1 g SA was dissolved in 50 ml deionized water, and the mixture was stirred overnight to obtain a homogeneous 2% (w/w) SA solution. Then, 0.975 g MES was added into the SA solution, and pH of the solution was adjusted to 5.5 with 1 M sodium hydroxide solution. 57.5 mg NHS and 191.7 mg EDC (at a molar ratio of 1:2) were added to the solution to activate carboxy groups. After 1 h, a certain amount of DFO was added into the solution and the reaction continued for 24 h at room temperature. Finally, the obtained solution was put into a dialysis bag with a molecular weight cut-off of 7 kDa and dialyzed for 5 days to remove unreacted DFO and excess MES, EDC and NHS. Acquired products were named as G-DFO-SA.

^{1}H Nuclear Magnetic Resonance Spectroscopy was conducted to confirm the graft of DFO onto SA. For preparing the samples, SA and G-DFO-SA were dissolved in deuteroxide firstly. Then, the solutions were detected with a 600 M Nuclear Magnetic Resonance (Avance III, Burker,

German) and the spectra were recorded by the equipment.

2.4. Preparation and component optimization of hydrogels

2.4.1. Preparation of hydrogels

Hydrogels were prepared according to methods adapted from the procedures reported in previous study [17]. Briefly, 2% precursor solution of SA and G-DFO-SA were prepared by dissolving 1 g SA or G-DFO-SA powder into 50 ml deionized water. Then, 1 ml precursor solution, 30 mg GDL, and 10 mg BG powders were mixed in a syringe and the mixture was repeatedly pipetted 20 times to form a homogeneous solution which was subsequently injected into a customized cylindrical mold. After the solution was injected into a mold, the calcium ions were released from the BG powders under the weak acidic environment created by GDL and the SA as well as G-DFO-SA molecules started to crosslink. After 45 seconds, the solution was converted into hydrogels in the mold.

In order to obtain a proper graft ratio of DFO to SA, three different input ratios of DFO and SA, including 10 mg DFO/1 g SA, 50 mg DFO/1 g SA, and 250 mg DFO/1 g SA, were applied, and their products were labeled as G-1% DFO-SA, G-5% DFO-SA, and G-25% DFO-SA, respectively. Then, these three kinds of G-DFO-SA materials were used to prepare hydrogels. Therefore, totally four different hydrogels were prepared, which were marked as SA/BG, G-1% DFO-SA/BG, G-5% DFO-SA/BG, and G-25% DFO-SA/BG, respectively. The labels and compositions of different hydrogels were concluded as Table 1.

2.4.2. Biocompatibility assessment of hydrogels

Hydrogel extracts were prepared according to the procedures reported in a previous literature [22]. Briefly, 1 cm^3 of hydrogels were placed in a cell culture dish with a diameter of 6 cm. Then, 10 ml of ECM or DMEM was added into the dishes and the dishes were placed in the cell incubator for 24 h. At the end of the incubation, the solution was taken out of the dishes, centrifuged at 1000 rpm (Cence L530) to remove hydrogels debris, and filtered with a 0.22 μm filter to sterilize the solution. The solution, which was regarded as hydrogel extract, was stored in 4 °C for further use.

Cell Counting Kit-8 (CCK8) assay was adopted to evaluate the biocompatibility of hydrogels. Original hydrogel extracts were diluted with ECM or DMEM at a ratio of 1/16. Then, diluted extracts of SA/BG, G-1%DFO-SA/BG, G-5%DFO-SA/BG, and G-25%DFO-SA/BG hydrogels were applied to culture cells, while cells cultured with the normal culture medium were regarded as controls. Specifically, HUVECs or HDF cells were seeded at a density of $1*10^4$ cells per well in a 48-well plate and cultured with the normal culture medium for 12 h. Then, the cell culture medium was discarded and 200 μl of serum-free medium containing 10% CCK8 solution was added into each well. After that, the cells were further incubated with the CCK8 solution for 90 min. Then, 100 μl of supernatant was taken out from each well and transferred to a well of a 96-well plate and the OD value of the supernatant at 450 nm was recorded with a microplate reader (Synergy 2, Bio-TEK). OD value at 12 h was regarded as day 0. Meanwhile, after the supernatant was taken out from the cell culture wells, residual CCK8 solution in each well was then replaced with normal medium or diluted hydrogel extracts to further culture cells. OD values at day 1, day 2, and day 3 were obtained as same as day 0.

Table 1
Compositions of hydrogels and corresponding label.

Quality of sodium alginate	Quality of deferoxamine	Integration pattern	Label
1g	10 mg	Chemical grafting	G-DFO-1% SA/BG
1g	50 mg	Chemical grafting	G-DFO-5% SA/BG
1g	250 mg	Chemical grafting	G-DFO-25% SA/BG
1g	50 mg	Physical encapsulation	F-DFO-SA/BG

2.4.3. In vitro angiogenesis assessment of hydrogels

The angiogenesis function of the hydrogels was assessed by a Matrigel-based method. Firstly, 100 μl growth factor reduced Matrigel (Corning, USA) was transferred to a well of a 48-well plate and the solution of Matrigel was incubated at 37 °C for 1 h to form a gel substrate in the wells. Then, HUVECs in the logarithmic growth phase were digested and resuspended with ECM at a density of $6*10^5$. Finally, 50 μl HUVEC suspension was added on the Matrigel and 150 μl ECM or different kinds of hydrogel extracts were used to culture the cells. The cells cultured with ECM were regarded as the control, and the cells treated with extracts of SA/BG, G-1%DFO-SA/BG, G-5%DFO-SA/BG hydrogels were named as SA/BG, G-1%DFO-SA/BG, G-5%DFO-SA/BG, respectively. After being cultured for 6 h, the cells on the Matrigel were observed with an optical microscope (Leica DMI 3000B, Germany) and images were taken with a CCD camera (Leica DFC 420C) camera connected with the microscope. The obtained images were processed by ImageJ software and the circles and junctions formed by the cells were manually counted.

2.5. Characterization of optimized hydrogels

2.5.1. Morphological characteristics of hydrogels

Based on the results of biocompatibility and stimulatory effects on angiogenesis at section 2.4, G-5%DFO-SA/BG was selected for all subsequent experiments. For convenience, G-5%DFO-SA/BG was renamed as G-DFO-SA/BG in all following experiments. In addition, in order to compare the release behaviors of DFO grafted with SA or freely encapsulated within a hydrogel, a SA/BG hydrogel containing free DFO was fabricated. This hydrogel was prepared with the same method used for preparing the SA/BG hydrogel except that the SA precursor was mixed with DFO (5%) in advance. The obtained hydrogel was named as F-DFO-SA/BG.

The interior structure of SA/BG, F-DFO-SA/BG, and G-DFO-SA/BG hydrogels were characterized by scanning electron microscopy (SEM) with a scanning electron microscope (Hitachi S-4800, Japan). The as-obtained hydrogels were put into a lyophilizer (BETA1-8, German) and lyophilized for 48 h. Then, the lyophilized sponges were cut along the longitudinal direction and the cross-section was sputter-coated with a thin layer of gold. Finally, the interior structure was directly visualized and photographed with the scanning electron microscope.

2.5.2. Mechanical testing

The stress-strain curve and elastic modulus of SA/BG, F-DFO-SA/BG, and G-DFO-SA/BG hydrogels were acquired with an electronic universal testing machine (Zwick/Roell Z020). Briefly, hydrogels with a diameter of 6 mm and a height of 10 mm were prepared. Then, hydrogels were placed on the test platform and the compression speed was set to 1 mm/min. The test kept continuing until hydrogels were broken. Elastic modulus was acquired according to the linear portion of the stress-strain curve.

2.5.3. Evaluation of DFO in vitro release behaviors

To evaluate the DFO in vitro release behavior of F-DFO-SA/BG and G-DFO-SA/BG, 1 cm^3 hydrogel was immersed in 10 ml deionized H_2O in a 6-well plate and incubated under 37 °C. At fixed interval (12 h, 24 h, 48 h, 84 h, 120 h,168 h), 1 ml of supernatant were taken out and 1 ml fresh deionized H_2O were replenished. The amount of DFO in the supernatant was detected as previously reported [31]. Briefly, $FeCl_3$ was dissolved in deionized H_2O (0.01 M). Then, the collected supernatant and $FeCl_3$ solution were mixed at 1:1(v/v) in a centrifuge tube. The absorbance of the mixture solution at 485 nm wavelength was measured using a UV–vis spectrophotometer (Tecan infinite m200pro). Finally,

the amount of released DFO was calculated according to the standard DFO calibration curve.

2.6. In vitro degradation evaluation of hydrogels

The initial weights of SA/BG, F-DFO-SA/BG, and G-DFO-SA/BG hydrogels were weighed and described as W_0. Then, 1 cm^3 hydrogels were immersed in 5 ml phosphate buffered saline (PBS) and placed in a shaker at 37 °C and shaken at a speed of 60 rpm/min. At pre-set time intervals (day 1, day 3, day 5, day 7, day 10, and day 14), hydrogels were taken out from PBS and the water on the hydrogel surface was wiped off. Then, the hydrogels were photographed and weighed to record their morphology change and mass change with time, respectively. The weight of the hydrogel at pre-set time intervals was described as W_t. The mass change was calculated according to the following equation:

$$\text{Mass change } (\%) = (W_t - W_0)/W_0 \times 100$$

The interior structure changes of SA/BG, F-DFO-SA/BG, and G-DFO-SA/BG hydrogels was characterized by SEM. Briefly, hydrogels were collected after being immersed in PBS for different periods. Then, the hydrogels were lyophilized before they were observed with SEM. Samples for SEM characterization were prepared according to the methods described in 2.5.1. The average pore size in the lyophilized hydrogels was measured by Image J.

In addition, mechanical property changes are also indicators of material degradation. After being immersed in PBS for 5 days, SA/BG, F-DFO-SA/BG, and G-DFO-SA/BG hydrogels were collected and characterized by mechanical tests according to the methods described in 2.5.2.

Furthermore, the release behavior of calcium ions from SA/BG, F-DFO-SA/BG, and G-DFO-SA/BG hydrogels during the degradation period was evaluated. Briefly, the supernatant of the soaking medium of different hydrogels was collected at different time points and the concentration of calcium ions in the different supernatant was detected by inductively coupled plasma optical (iCAP7600, Thermo, America).

2.7. Effects of hydrogels on inducing cell infiltration in vitro

To evaluate the effects of hydrogels on inducing cell infiltration in vitro, transwell migration assay was conducted to estimate the effects of BG and DFO on the migration of HDF cells and HUVECs. Briefly, HDF cells or HUVECs resuspended with DMEM or ECM at a density of $3*10^5$ cells per ml and 100 μl cell suspension was added in the upper chamber of a 24-well transwell plate (Corning; pore size = 8 μm). After 12 h, different media was added into the lower chamber of the transwell plate with different purposes and normal cell culture medium was added to the lower chamber as the control. The effects of BG on cell migration were evaluated by adding extract of SA/BG hydrogel into the lower chamber. In addition, to evaluate the effects of DFO on cell migration, serum-free DMEM or ECM containing DFO was added into the lower chamber. The serum-free DMEM or ECM containing DFO was obtained by dissolving a certain amount of DFO powder in serum-free DMEM and ECM. The concentration of DFO was determined according to the DFO release curve of G-DFO-SA/BG hydrogel at section 2.5.3. Furthermore, to evaluate the synergistic effects of BG and DFO on cell migration, the extract of G-DFO-SA/BG hydrogel was added into the lower chamber.

After 24 h, transwells were taken out and the medium in the upper chamber was discarded. Then, cells were fixed by immersing transwells in 4% paraformaldehyde for 30 min before they were stained with 0.5% crystal violet for 30 min. Finally, the cells in the upper side of the transwell membrane were removed by a cotton swab and the cells migrated to the down side of the tranwell membrane were photographed by using an optical microscope. Five images were captured for each sample and the stained cells were counted manually.

2.8. Evaluation of the degradation behavior of hydrogels and tissue infiltration in vivo

All animal experiment protocols were approved by the Institutional Review Committee of Shanghai Jiao Tong University, School of Biomedical Engineering. The approval number was 2019008. In this animal study, thirty-six female BALB/c mice aged 8 weeks were randomly divided into three groups. Mice were anesthetized with 4% chloral hydrate (0.01 ml/g). Once the mice were under deep anesthesia, the hair on the dorsal was shaved with a razor, and skin was sterilized with alcohol cotton swaps. Then, a 5 mm incision in length was cut on the back of a mouse and 150 μl hydrogel solution was injected into the incision with a syringe. Finally, the incision was closed with a degradable suture and sterilized with alcohol cotton swaps again. Tissue samples were collected on the 3rd, 7th, 14th, and 21st days post-surgery. Collected samples were fixed in paraformaldehyde for 48 h firstly. Then, samples were embedded in paraffin and sectioned with a microtome (Leica RM2245) into 5 μm thick slides. Finally, hematoxylin & eosin (HE) staining was performed for evaluating tissue infiltration and investigating hydrogel degradation. Remained hydrogel and infiltrated cells in the stained sections were observed with an optical microscope and images were taken with a CCD camera (Leica DFC 420C) connected with the microscope.

2.9. Evaluation of wound healing ability of hydrogels in a rat full-thickness excision model

All animal experiment protocols were approved by the Institutional Review Committee of Shanghai Jiao Tong University, School of Biomedical Engineering. The approval number was 2019008. In this animal study, twenty-four male Sprague Dawley rats aged 8 weeks were randomly divided into 4 groups. The rats were anesthetized with 10% chloral hydrate (1 ml/250 g). The hair on the dorsal was shaved with a razor, and skin was sterilized with alcohol cotton swaps. Two full-thickness excisions with a diameter of 15 mm were made on each rat. For the control group, the wounds were treated nothing and were dressed by using medical gauze and bandage directly. The wounds treated with 500 μl of SA/BG, F-DFO-SA/BG, or G-DFO-SA/BG hydrogels were named as SA/BG, F-DFO-SA/BG, and G-DFO-SA/BG, respectively. At pre-determined intervals (day 7, day 10, and day 14), the wounds were photographed and the remained wound area was measured by ImageJ software. Then, wound closure was calculated by the following formula:

$$\%\ \text{wound closure} = (A_0 - A_t)/A_0 \times 100$$

where A_0 is the surface of the wound area at day 0 and A_t is the surface of the wound area at day7, day 10, and day 14, respectively.

In addition, three rats were sacrificed on day 7 and day 14 for each group, and tissue was incised and fixed in 4% paraformaldehyde for 48 h. Then, samples were dehydrated in gradient ethanol and embedded in paraffin before they were sectioned into 5 μm thick slides for subsequent histological analysis. HE staining was performed on the samples collected on day 14 according to the methods described in section 2.7 to confirm re-epithelialization of different wounds at day 14. Masson trichrome was conducted on the samples collected on day 14 to evaluate the collagen deposition and maturity in the wounds treated with different materials at day 14. Concisely, slides were dewaxed in xylene and hydrated in gradient alcohols. Then, slides were stained under the guidance of the Masson's Trichrome Stain Kit (Solaribo, China).

The neovascularization and mature vessels in the regenerated tissue at day 7 were visualized by co-immunofluorescence staining of platelet endothelial cell adhesion molecule-1 (CD31) and alpha-smooth muscle actin (α-SMA). Briefly, slides were dewaxed in xylene and hydrated in gradient alcohols and PBS. The antigen in the samples was repaired by heating the slides for 20 min in 0.01 M sodium citrate buffer. After

cooling down to room temperature, slides were rinsed three times with PBS and blocked with 5% BSA/PBS solution for 1 h at 37 °C. Then, the slides were incubated with primary antibody cocktail solution containing rabbit anti-CD31 (ThermoFisher Scientific, USA, diluted with 1% BSA at ratios of 1/100) and mouse anti-α-SMA (Abcam, UK, diluted with 1% BSA at ratios of 1/2000) overnight at 4 °C. Then, the slides were rinsed with PBS for three times before they were incubated with secondary antibody solution containing Alexa 488 goat anti-rabbit IgG (Invitrogen, USA, diluted with 1% BSA at ratios of 1/300) and Alexa 594 goat anti-mouse IgG (Invitrogen, USA, diluted with 1% BSA at ratios of 1/300) for 1 h at 37 °C. Finally, slides were rinsed with PBS for three times before they were mounted with DAPI Fluoromount-GTM (Yeasen, China). Then, the sections were observed and images were captured with a confocal laser scanning microscope (Leica SP5, Germany).

Immunohistochemistry of VEGF and HiF-1α was conducted to verify the mechanism of neovascularization. After the samples were processed according to the methods described in the above section and slide sections of samples were obtained, the slides were further processed with 0.3% hydrogen peroxide in methyl alcohol for 30 min to block the endogenous peroxidase. After blocking with 5% BSA/PBS, slides were incubated with primary antibodies of rabbit anti-VEGFA(Abcam, UK, diluted with 1% BSA at ratios of 1/1000) or mouse anti-Hif-1α (ThermoFisher Scientific, USA, diluted with 1% BSA at ratios of 1/500) overnight at 4 °C. Then, slides were incubated with the HRP-conjugated goat anti-rabbit secondary antibodies or HRP-conjugated goat anti-mouse secondary antibody (Abcam, UK, diluted with 1%BSA at ratios of 1/2000) for 1 h at 37 °C. Finally, the slides were stained with a DAB substrate kit (Abcam, UK) and cell nucleus was stained in hematoxylin solution for 1 min. Stained images were captured by an optical microscope and the ratio of VEGF or Hif-1α positive area was measured by ImageJ software.

2.10. Statistical analysis

All data were described as mean ± standard deviation ($n \geq 3$). Statistics were analyzed using IBM SPSS 19.0 statistics. One-way ANOVA were used for statistical analysis of multiple comparisons. The values $^{*}p < 0.05$, $^{**}p < 0.01$, and $^{***}p < 0.001$ indicated as statistical difference,

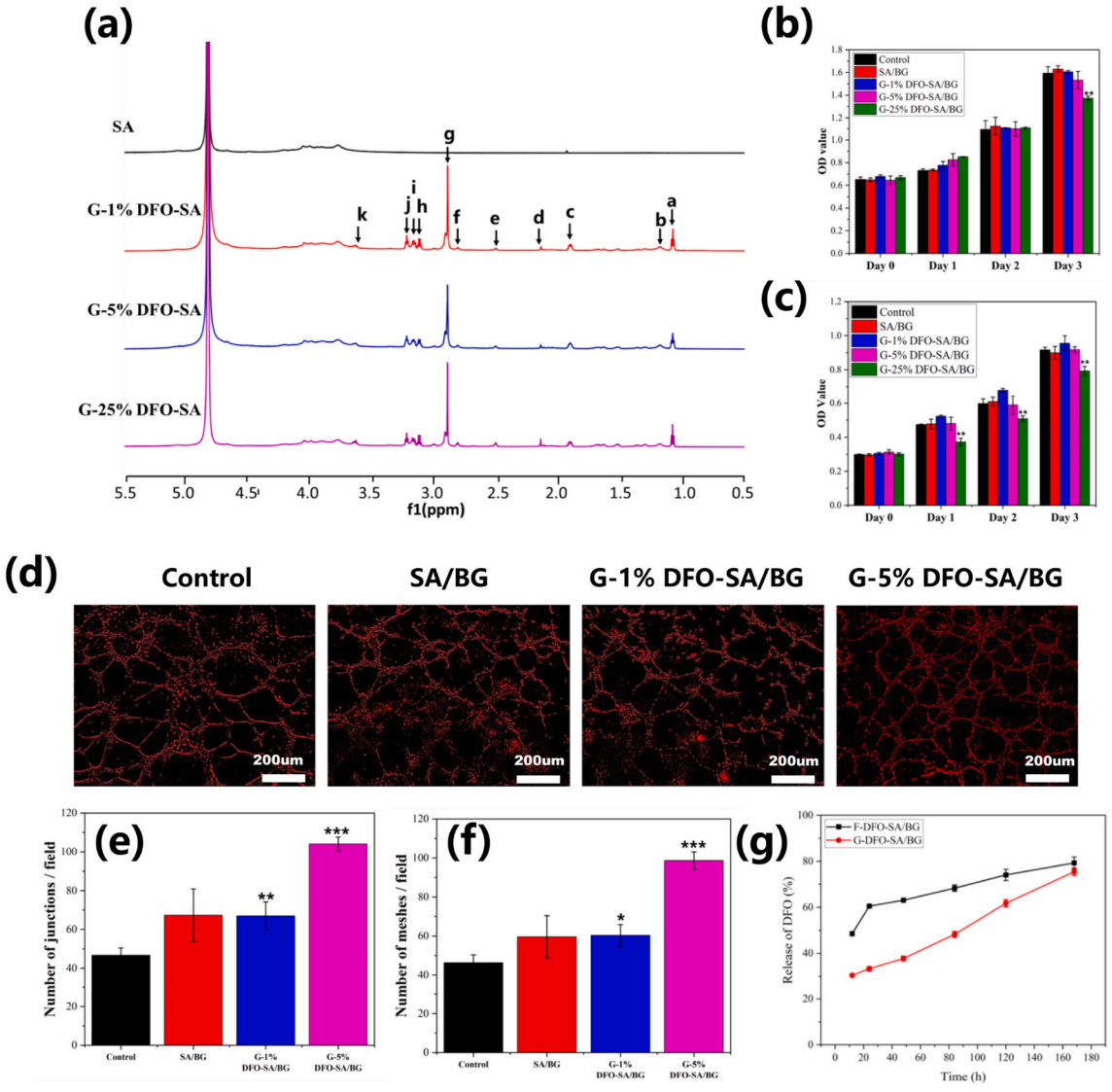

Fig. 1. Characterization of grafted SA and component optimization of hydrogels. (a) 1HNMR of SA, G-1%DFO-SA, SA, G-5%DFO-SA and SA, G-25%DFO-SA. (b) and (c) Effects of hydrogels extracts on proliferation of HDF cells and HUVECs, respectively. (d) Effects of different hydrogel extracts on in vitro vascularization of HUVECs cultured on Matrigel. (e) and (f) Quantitative analysis of meshes and junctions formed in the in vitro vascularization assay by HUVECs cultured on Matrigel with control culture medium or different hydrogel extracts, respectively. (g) Release curves of DFO from F-DFO-SA/BG and G-DFO-SA/BG hydrogels. All data are compared with Control. * represents $p < 0.05$, ** represents $p < 0.01$ and *** represents $p < 0.001$.

significant statistical difference, and very significant statistical difference, respectively.

3. Results and discussion

3.1. Synthesis and characterization of DFO grafted SA

DFO was grafted onto the SA through amidation reaction under the catalysis of EDC and NHS. ^{1}HNMR spectra of SA and DFO-SA are shown in Fig. 1a. Compared to the spectra of SA, there were some new peaks in the spectra of all DFO-SA, which were consistent with the characteristic peaks of DFO reported in previous studies [32]. Particularly, a new peak at 2.123 ppm (^{d}H) was consistent with methyl protons (-CH_3), ^{e}H (2.50 ppm) and ^{g}H (2.88 ppm) belonged to the methylene protons between two carbonyl groups (-CO-CH_2-CH_2-CO-). In addition, ^{f}H (2.79 ppm) and ^{h}H (3.10 ppm) were assigned to methylene protons next to -NH- group (-NHCH_2-), and ^{k}H (3.61 ppm) belonged to methylene protons next to -N-OH group (-NOH-CH_2-). All these results indicated that DFO was successfully grafted onto the SA.

3.2. Component optimization of hydrogels

The effects of different hydrogels on the proliferation of HDF cells and HUVECs were shown in Fig. 1b and c, respectively. Fig. 1b shows that the extracts of SA/BG, G-1%DFO-SA/BG and G-5%DFO-SA/BG hydrogels had similar biocompatibility to the normal culture medium (Control) regarding their effects on the proliferation of HDF cells. However, when the ratio between DFO and SA was 250 mg DFO/1g SA, the extract of the hydrogel (G-25%DFO-SA/BG) showed obvious inhibitory effects on the proliferation of HDF cells at day 3. Similarly, these hydrogels showed good biocompatibility to the proliferation of HUVECs, except the extract of the hydrogel (G-25%DFO-SA/BG) that inhibited the growth of HUVECs all the time (Fig. 1c). The cytotoxicity of the G-25% DFO-SA/BG hydrogel may be caused by the high concentration of DFO in the extract [28]. Considering that biocompatibility is a prerequisite for a biomaterial used for tissue regeneration, G-25%DFO-SA/BG hydrogel was not used in the following experiments.

The effects of different hydrogels on in vitro vascularization of HUVECs was investigated and the results are shown in Fig. 1d, e and f. It can be seen from the representative images of HUVECs in Fig. 1d that, when HUVECs were cultured on the Matrigel with the extracts of G-1% DFO-SA/BG hydrogel or G-5% DFO-SA/BG hydrogel, more HUVECs tended to migrate and self-assembled into capillary-like networks as compared to those cultured with ECM (Control). Statistical analysis was further carried out on the vascularization images and the mesh formation and junction formation by HUVECs cultured with different media was shown in Fig. 1e and f, respectively. Although SA/BG hydrogel improved the average number of meshes and junctions as compared to the normal culture medium (Control), there was no significant difference. Interestingly, there were significantly more meshes and junctions formed by the HUVECs cultured with the extracts of G-1%DFO-SA/BG and G-5%DFO-SA/BG hydrogels compared to those formed by the HUVECs cultured with ECM. Furthermore, HUVECs under the stimulation of G-5%DFO-SA/BG hydrogel extract formed a higher number of meshes and junctions compared to those cultured with G-1%DFO-SA/BG hydrogel extract. Since tissue regeneration would benefit a lot from angiogenesis [33], G-5%DFO-SA/BG hydrogel showed advantages over other hydrogels for wound healing.

In summary, the G-5% DFO-SA/BG hydrogel possessed both good biocompatibility and strong stimulatory effects on vascularization of endothelial cells and it was selected for all further studies. In the following experiments, this hydrogel was named as G-DFO-SA/BG hydrogel for convenience.

3.3. DFO release behaviors from hydrogels

Release curves of DFO from F-DFO-SA/BG and G-DFO-SA/BG hydrogels were presented in Fig. 1g. There was a burst release of DFO from F-DFO-SA/BG hydrogel in the first 24 h while the G-DFO-SA/BG hydrogel achieved the sustained release of DFO within 7 days. The release curve of G-DFO-SA/BG hydrogel was almost linear ($R^2 = 0.992$) from 12 h to 168 h while there was a sharp increase from 12 h to 24 h in the release curve of F-DFO-SA/BG hydrogel. Specifically, the amount of released DFO from F-DFO-SA/BG hydrogel was up to 60.5% in the first 24 h, but only 33.4% DFO was released from the G-DFO-SA/BG hydrogel.

3.4. Characterization and degradation of hydrogels

Photos of as-obtained SA/BG hydrogel, F-DFO-SA/BG hydrogel, and G-DFO-SA/BG hydrogel are shown in the first row (Day 0) of Fig. 2a. It can be seen that all hydrogels could be injected into a mold to form a cylindrical shape and there was no difference in the appearance of hydrogels.

The degradation behavior of hydrogels was characterized by mass loss, internal structure transformation and mechanical disintegration. Fig. 2a shows the macroscopic photographs of hydrogels after being soaked in PBS for a certain period. Before day 5, all hydrogels kept their typical cylindrical shape. At day 7, G-DFO-SA/BG hydrogel could not maintain a cylindrical shape and this change kept until the cylindrical hydrogel totally lost its shape at day 14. However, there was no obvious shape change of SA/BG hydrogel until day 14 when the SA/BG hydrogel lost its cylindrical shape and F-DFO-SA/BG hydrogel did not show obvious shape changes during the whole degradation experiment. Mass of SA/BG hydrogel and F-DFO-SA/BG hydrogel kept rising all time because of their swelling (Fig. 2c). In contrast, mass change of G-DFO-SA/BG hydrogel could be divided into two stages. In the first 7 days, the mass of the G-DFO-SA/BG hydrogel slowly increased, which was like that of the other two hydrogels. However, the mass of the G-DFO-SA/BG hydrogel started to decrease on day 10, and only 48% of the original weight was maintained at day 14.

Fig. 2b shows the transformation of the internal structure of hydrogels during the degradation process. After the hydrogels were immersed in PBS for 3 days, pores of the hydrogels swelled and became larger than those of the as-obtained hydrogels (day 0). On day 5, G -DFO-SA/BG hydrogel lost its porous structure and was not porous (NP) while the other two hydrogels still maintained the porous structure with swelled pores. On day 10, SA/BG hydrogel lost its porous structure and became not porous and only F-DFO-SA/BG hydrogel maintained porous structure with slightly decreased pore size. At the end of the degradation experiment (day 14), all hydrogels became not porous. The statistical analysis on the mean pore size measured from SEM images was shown in Fig. 2d, which showed a consistent trend of pore size changes with the images. Specifically, swelling of the pores on day 3 could be obviously observed as the average pore size of SA/BG, F-DFO-SA/BG, and G-DFO-SA/BG hydrogels increased from 180 μm, 142 μm, and 116 μm–281 μm, 219 μm, 202 μm, respectively. The porous structure disappearance in G-DFO-SA/BG hydrogel on day 5 and in SA/BG hydrogel on day 10 was also reflected in the graph.

Stress-strain curves of as-obtained hydrogels (solid lines) are shown in Fig. 3a. Obviously, F-DFO-SA/BG hydrogel had the highest yield stress among the three types of hydrogels, followed by the SA/BG hydrogel, and the G-DFO-SA/BG hydrogel had the lowest yield stress. According to these stress-strain curves, the elastic modulus of SA/BG, F-DFO-SA/BG, and G-DFO-SA/BG hydrogels was obtained as 0.49 MPa, 0.68 MPa, and 0.06 MPa, respectively (Fig. 3b). The high mechanical properties of F-DFO-SA/BG hydrogel may be attributed by the newly formed hydrogen bond formation between DFO and SA [34]. The amine and carbonyl groups on the DFO could form hydrogen bond with the hydroxyl groups on the SA. Reduced crosslinking density in the hydrogel

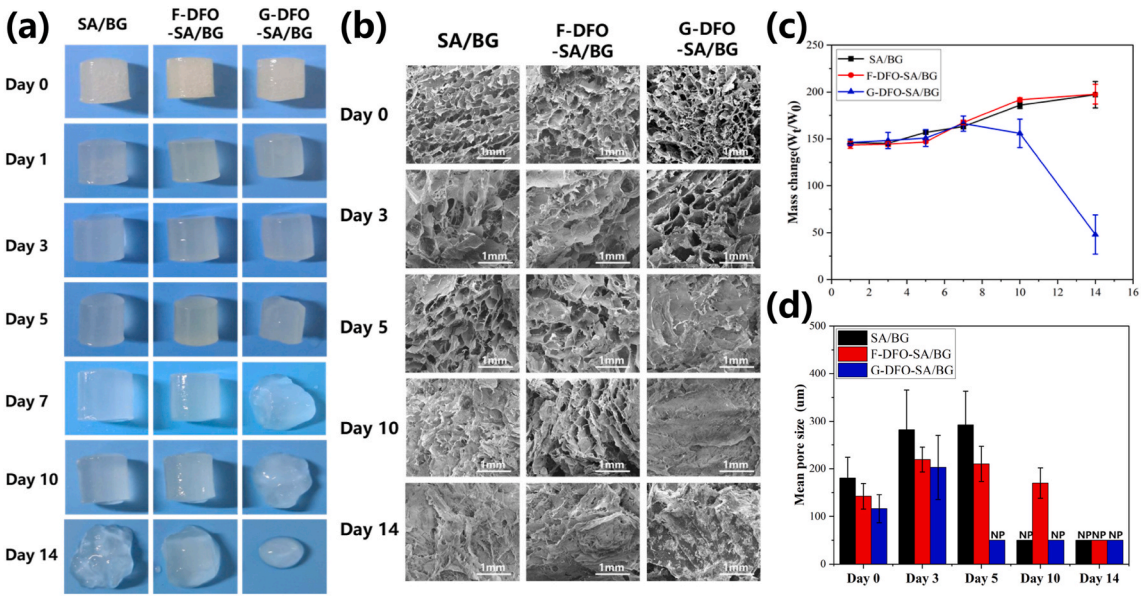

Fig. 2. Characterization and degradation of SA/BG hydrogel, F-DFO-SA/BG hydrogel, and G-DFO-SA/BG hydrogel. (a) Macroscopic photographs of as-obtained hydrogels (day 0) and the hydrogels during degradation on day 3, day 5, day 7, day 10, day 14. (b) Representative images of interior structure of as-obtained hydrogels (day 0) and the hydrogels during degradation on day 3, day 5, day 10, day 14. (c) Quantitative analysis of mass change of hydrogels with degradation time. (d) Statistics of mean pore size measured from the representative SEM images. NP means not porous.

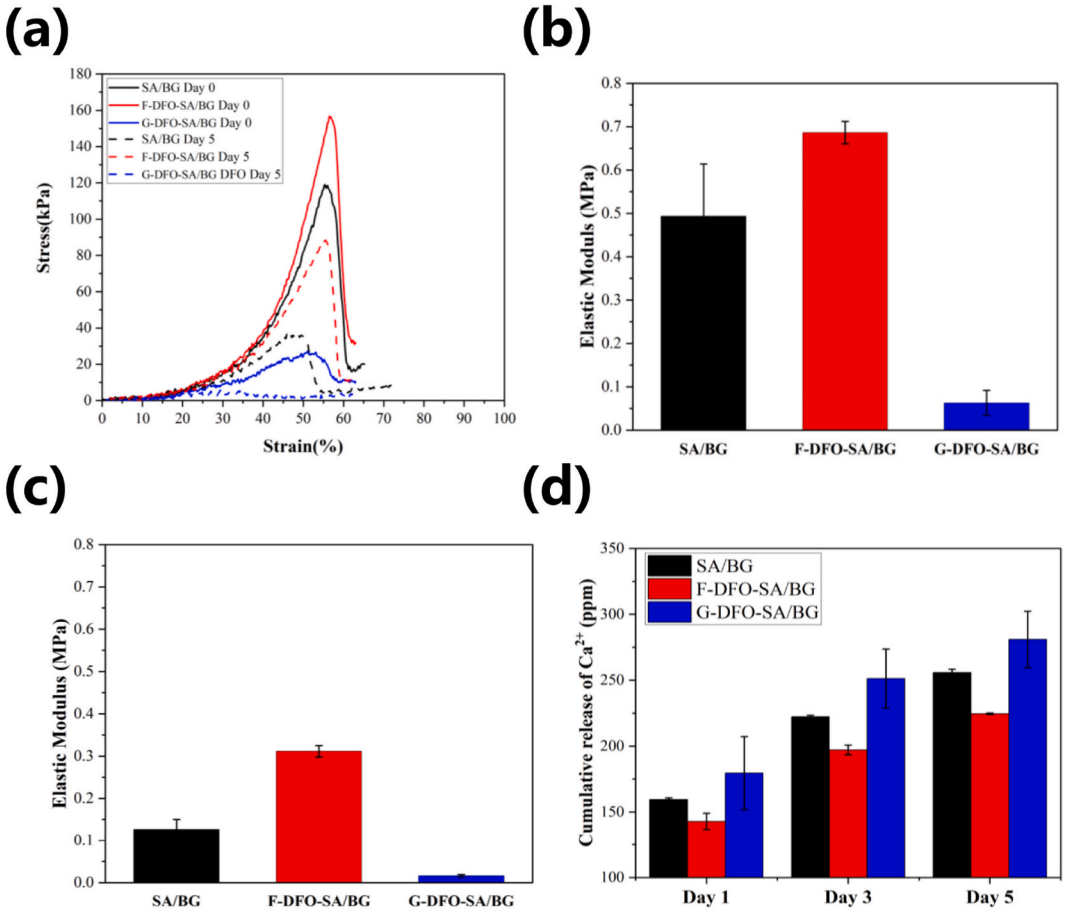

Fig. 3. Characterization and degradation of SA/BG hydrogel, F-DFO-SA/BG hydrogel, and G-DFO-SA/BG hydrogel. (a) Stress-strain curve of hydrogels before (solid lines) and after (dotted lines) immersing in the PBS for 5 days. (b) Elastic modulus of as-obtained SA/BG, F-DFO-SA/BG, and G-DFO-SA/BG hydrogels. (c) Elastic modulus of SA/BG, F-DFO-SA/BG, and G-DFO-SA/BG hydrogels after immersing in the PBS for 5 days. (e) Cumulative release of Ca^{2+} from different hydrogels.

could be an explanation for the decreased mechanical properties of G-DFO-SA/BG [35].

After the hydrogels were immersed in PBS for 5 days, the mechanical strength of all hydrogels significantly declined as compared to those of as-obtained hydrogels, shown by their stress-strain curves (dotted lines) (Fig. 3a). Specifically, the elastic modulus of G-DFO-SA/BG hydrogel dropped from 0.06 MPa to 0.01 MPa (Fig. 3c), which indicated that the G-DFO-SA/BG hydrogel almost disintegrated as about 83% mechanical strength was lost. The elastic modulus of F-DFO-SA/BG hydrogel decreased from 0.68 MPa to 0.31 MPa, showing a 50% decrease while the elastic modulus of SA/BG hydrogel showed a 75% lost (0.49 MPa–0.13 MPa).

The cumulative calcium ion release from all hydrogels was shown in Fig. 3d. G-DFO-SA/BG hydrogel showed the fastest ion release rate among all hydrogels, followed by the SA/BG hydrogel, while calcium ion release from F-DFO-SA/BG hydrogel was the slowest. Specifically, on day 1, the amount of calcium ion released from G-DFO-SA/BG hydrogel was 179 ppm, while SA/BG hydrogel only released 159 ppm calcium ions and only 142 ppm calcium ions were released from F-DFO-SA/BG hydrogel. On day 3, the amount of released calcium ion from G-DFO-SA/BG hydrogel, SA/BG hydrogel and F-DFO-SA/BG hydrogel increased to 251 ppm, 229 ppm and 197 ppm, respectively. At the last test point (day 5), total 281 ppm calcium was released from G-DFO-SA/BG hydrogel. As a contrast, cumulative calcium ion release from SA/BG hydrogel and G-DFO-SA/BG hydrogel was 262 ppm and 224 ppm, respectively. Trends of calcium ion release from SA/BG, F-DFO-SA/BG, and G-DFO-SA/BG hydrogels were completely consistent with the trends of mass change, transformation of internal structure and mechanical strength changes. The reason for fast calcium ion release from G-DFO-SA/BG hydrogel may be that the grafting expended the carboxyl groups on the SA, thus decreasing the number of crosslinking sites and allowing the calcium ions to diffuse faster from the network. In contrast, the slow release of calcium ions from F-DFO-SA/BG hydrogel resulted from the dense and double crosslinked network (hydrogen bond and ionic bond) in the hydrogel [36].

3.5. Effects of BG and DFO on cell migration

Effects of BG and DFO on cell migration were evaluated by a transwell model. HDF cells and HUVECs migrated into the down side of the transwell membrane were stained with crystal violet and the images are shown in Fig. 4a. Compared to the cells treated with ECM or DMEM, both HDF cells and HUVECs treated with SA/BG hydrogel extract or medium containing certain amounts of DFO showed an enhanced migration behavior. Interestingly, we found that DFO had a better migration promotion effect on HDF cells than BG while BG had a better migration promotion effect on HUVECs than DFO. Specifically, the number of migrated HDF cells stimulated by DFO contained DMEM was 79 per field, which was higher than that stimulated by SA/BG hydrogel extract (44 per field). Instead, the number of migrated HUVECs was 406 per field under the stimulation of BG compared to 312 per field under the stimulation of DFO. In addition, we found that BG and DFO could synergistically promote the migration of HDF cells and HUVECs as the number of migrated HDF cells and HUVECs was 130 and 518 per field, respectively, when they were cultured with the G-DFO-SA/BG hydrogel extract (Fig. 4b and c).

3.6. Degradation of hydrogels and tissue infiltration evaluation in vivo

Hydrogels were implanted in subcutaneous to evaluate their degradation in vivo and investigate the tissue infiltration into the hydrogels. According to the results shown in Fig. 5, G-DFO-SA/BG exhibited the best tissue infiltration and fastest degradation among all hydrogels and controls, which was consistent with the degradation behaviors of hydrogels in vitro. However, what differed from the in vitro degradation behaviors of hydrogels was that F-DFO-SA/BG showed faster degradation compared to SA/BG. Specifically, there were almost no cells inside the SA/BG and F-DFO-SA/BG hydrogels and there was a clear boundary (black dash line) between hydrogels and surrounding tissues at day 3 (Fig. 5a) and day 7 (Fig. 5b). However, a small number of cells (black arrows) had infiltrated into the G-DFO-SA/BG hydrogel and the

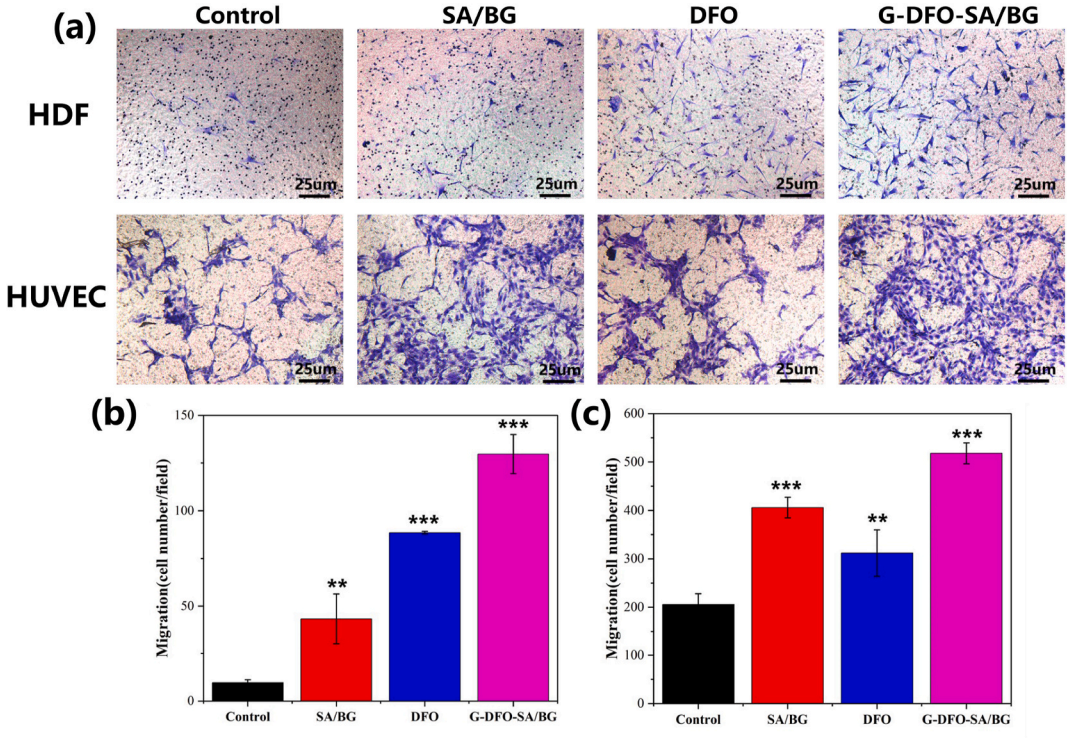

Fig. 4. Effects of BG and DFO on cell migration in vitro. (a) Transwell migration. (b) Statistics of the number of migrated HDF cells. (c) Statistics of the number of migrated HUVECs. All data are compared with Control. * represents $p < 0.05$, ** represents $p < 0.01$ and *** represents $p < 0.001$.

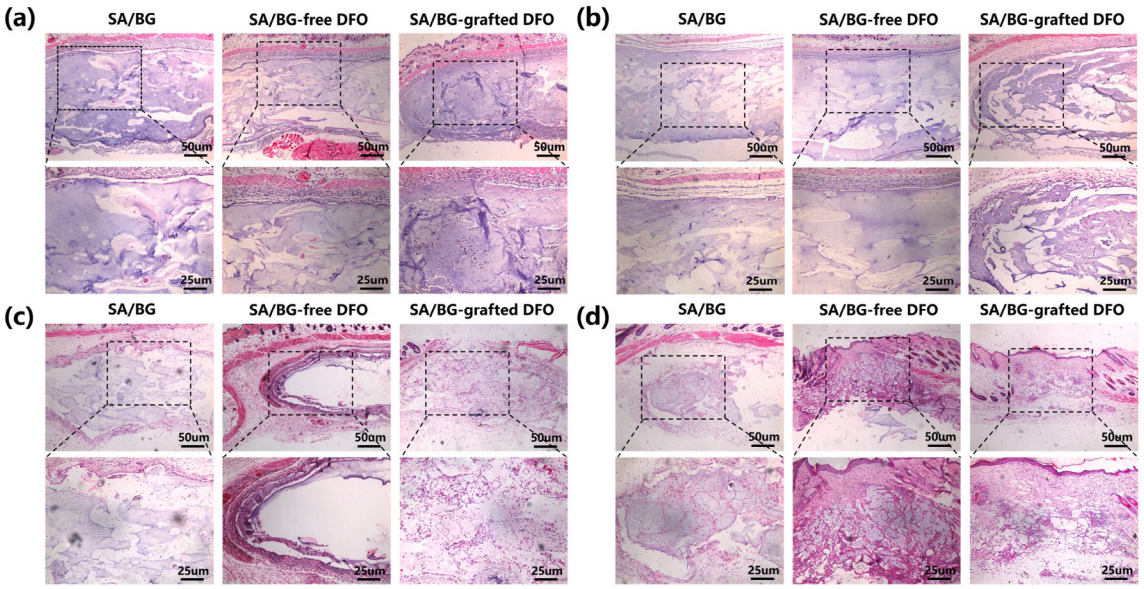

Fig. 5. Degradation of hydrogels and tissue infiltration evaluation in vivo. Representative HE stained images of SA/BG hydrogel, F-DFO-SA/BG hydrogel, and G-DFO-SA/BG hydrogel and surrounding tissues after being implanted in subcutaneous for 3 days (a), 7 days (b), 14 days (c), 21 days (d). T referrers to tissue; H referrers to hydrogel. Dash lines represent the boundary between hydrogel and tissue.

boundary between the hydrogel and surrounding tissues became blurred at day 7 (Fig. 5b). At day 14, there were still no cells entering into the SA/BG hydrogel, but a small number of cells had infiltrated to the edge of the F-DFO-SA/BG hydrogel (Fig. 5c). Besides, F-DFO-SA/BG hydrogel and surrounding tissue started to fuse at their interface. Interestingly, there were many cells in the inside of G-DFO-SA/BG hydrogel and the boundary between hydrogel and tissue disappeared. In addition, G-DFO-SA/BG hydrogel had also begun to degrade at day 14 since the purple area in the image had decreased significantly compared to the that in the image at day 3. A small number of cells were inside of SA/BG hydrogel while there were many cells in the F-DFO-SA/BG hydrogel at day 21 (Fig. 5d). At the same time, it can be observed that F-DFO-SA/BG hydrogel started to degrade. Excitingly, an obvious connective tissue network could be observed inside the G-DFO-SA/BG hydrogel, and the hydrogel almost completely degraded.

There are two reasons for the fast degradation and good tissue infiltration of G-DFO-SA/BG hydrogel. On the one hand, fast degradation could be attributed by the reduced crosslinking density. Degradation of hydrogel would allow cells to infiltrate into the inside of the hydrogel [37]. On the other hand, the infiltrated cells would accelerate the degradation of the hydrogel and they would form a virtuous circle [38]. Faster degradation and better tissue infiltration of F-DFO-SA/BG in comparison with SA/BG may be caused by the strong effects of the F-DFO-SA/BG hydrogel on promoting cell migration since DFO and BG had been proved to be able to synergistically promote cell migration in vitro (Fig. 4).

3.7. Wound closure and histological staining

Representative photographs of the wound healing process in the rat full-thickness excision model are shown in Fig. 6a. The process of wound healing was illustrated in Fig. 6b and the schematic diagram was obtained by using an arbitrary polygon tool in PowerPoint 2016 to trace the remained wound area in different time points according to the representative photos presented in Fig. 6a. It can be seen that the wound gradually closed over time (Fig. 6b), and wounds treated with hydrogels showed a significantly improved wound closure speed compared to the wounds treated with nothing (Control). The quantitative result of wound closure is presented in Fig. 6c, indicating that wounds treated with G-DFO-SA/BG hydrogel showed the fastest wound closure speed at the whole period among all wounds. At day 14, wounds treated with G-DFO-SA/BG hydrogel were almost completely closed (99%), while the closure rate of the wounds treated with nothing (Control), SA/BG hydrogel and F-DFO-SA/BG hydrogel was 92%, 96% and 97%, respectively. The re-epithelialization of the wound areas at day 14 was characterized by HE staining and representative images are presented in Fig. 6d. Obviously, the gap of un-epithelialization in the wounds treated with nothing (Control) was the largest (2.26 mm) among all gaps, which was much higher than that of the wounds treated with SA/BG hydrogel (1.76 mm), F-DFO-SA/BG hydrogel (1.64 mm) and G-DFO-SA/BG hydrogel (0.68 mm). A gap of un-epithelialization of 0.68 mm indicated that the wounds treated with G-DFO-SA/BG hydrogel almost had a complete epithelialization. In addition, Masson trichrome was conducted to assess the collagen deposition and the results are shown in Fig. 6e (low magnification) and Fig. 6f (high magnification). The blue color, which indicated the content of the collagen, was different in the stained tissue samples. Among all wounds treated with different conditions, those treated with G-DFO-SA/BG hydrogel possessed the highest amount of collagen since the images of the stained tissue samples in the G-DFO-SA/BG group showed the deepest blue color. Besides, wounds treated with F-DFO-SA/BG hydrogel and G-DFO-SA/BG hydrogel exhibited a more orderly collagen fiber arrangement than the wounds treated with nothing or SA/BG hydrogel. Mature collagen fibers (deep blue and oriented distribution) were presented at the wounds treated with G-DFO-SA/BG hydrogel. All these results indicated that G-DFO-SA/BG hydrogel had the best promotion effect on wound healing among all hydrogels.

3.8. Angiogenesis of wounds treated with hydrogels

Vascularization is an important phase in the wound healing process and it has been reported that vascularization had a positive influence on wound closure [39]. Neovascularization and mature vessels of wounds at day 7 were evaluated by immunofluorescence of CD31 and α-SMA. Representative images in Fig. 7a show that there were obviously more CD 31 positive (new formed) blood vessels and α-SMA positive (mature) blood vessels in the wounds treated with hydrogels than those in the wounds treated with nothing (Control). Furthermore, statistical analysis confirmed that the average number of CD 31 positive blood vessels in wounds treated with SA/BG, F-DFO-SA/BG and G-DFO-SA/BG hydrogel

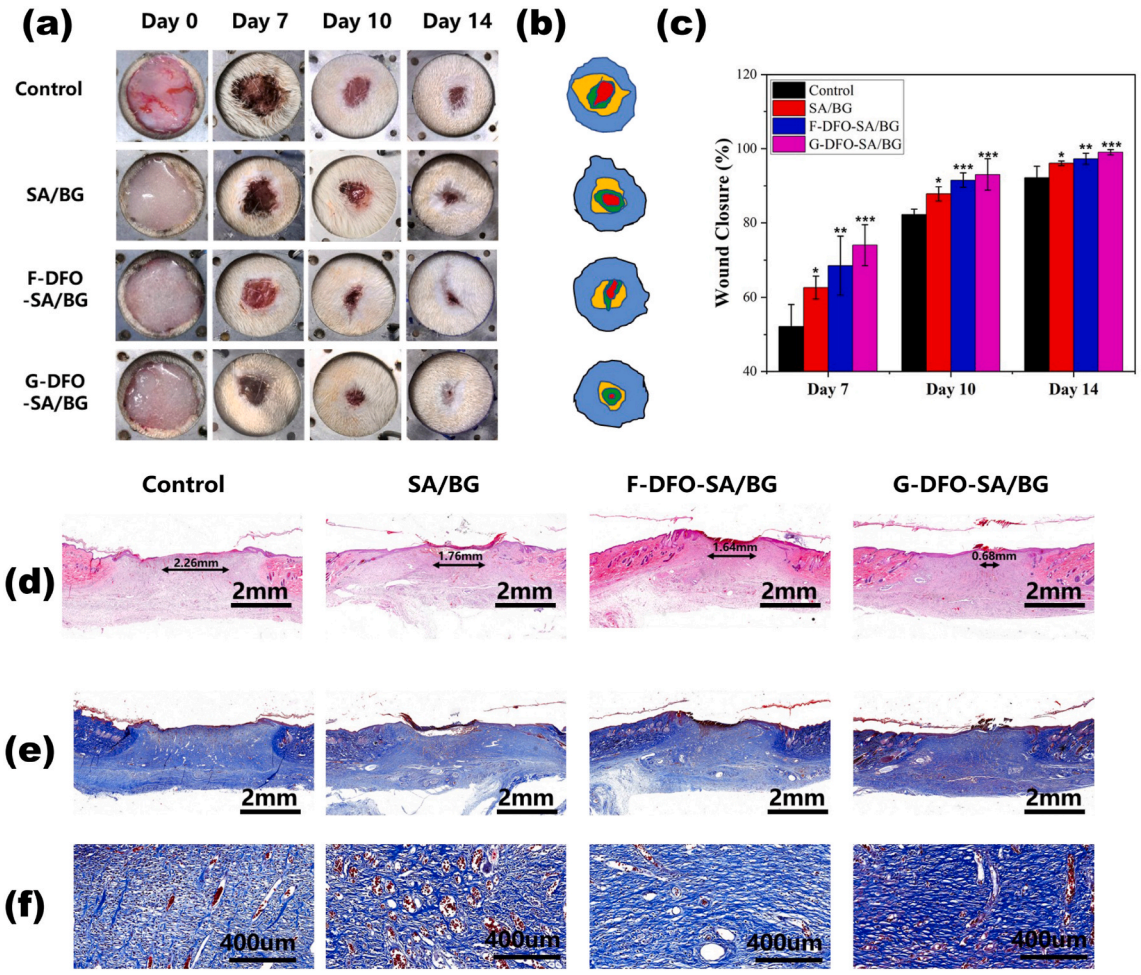

Fig. 6. In vivo assessment of hydrogels for wound healing. (a) Representative gross observation images of wounds treated with nothing (Control), SA/BG hydrogel (SA/BG), F-DFO-SA/BG hydrogel (F-DFO-SA/BG) and G-DFO-SA/BG hydrogel (G-DFO-SA/BG). (b) Schematic diagram of wounds treated with different materials. Blue area: the wound area at day 0; yellow area: the remained wound area at day 7; green area: the remained wound area at day 10; red area: the remained wound area at day14. (c) Quantitative analysis of wound closure rate at day 7, day 10, day 14. (d) HE stained images of wound tissue at day 14. (e) and (f) show the representative images of Masson trichrome stained wound tissue at day 14 taken at a low and high magnification, respectively. All data are compared with Control. * represents $p < 0.05$, ** represents $p < 0.01$ and *** represents $p < 0.001$.

was significantly higher than that in wounds treated with nothing (Control) ($p < 0.05$, $p < 0.05$, $p < 0.01$ respectively). Similarly, statistical analysis of α-SMA positive blood vessels is presented in Fig. 7c. The average number of mature blood vessels in wounds treated with F-DFO-SA/BG and G-DFO-SA/BG hydrogel was significantly higher than that in wounds treated with nothing (Control) ($p < 0.05$, $p < 0.001$ respectively). As to the wounds treated with SA/BG hydrogel, the average number of α-SMA positive blood vessels was higher than the number in wounds treated with nothing, but there was no significant difference ($p = 0.067$). In addition, whether it is CD31-positive blood vessels or α-SMA-positive blood vessels, the average number of wounds treated with G-DFO-SA/BG hydrogel was higher than the wounds treated with SA/BG and F-DFO-SA/BG hydrogel, which means wounds treated with G-DFO-SA/BG hydrogel presented the best vascularization.

The strong stimulatory effects of G-DFO-SA/BG hydrogel on angiogenesis could be explained from three aspects. Firstly, hydrogels containing BG and ion products of BG have been demonstrated to promote angiogenesis in our previous studies. BG contained hydrogel has been demonstrated to stimulate the polarization of macrophages into M2 and created an anti-inflammatory environment. Proper inflammation regulation could drive wound healing into the next phase [40]. In the latest study, we proved that BG could regulate the interactions between macrophages and repairing cells. BG activated macrophages were proved to recruit fibroblasts and endothelial cells both in vitro and in vivo. In addition, the extracellular matrix (ECM) synthesis of fibroblasts and vascularization of endothelial cells were enhanced in a full-thickness excisional model under the simulation of BG contained hydrogel [41]. Another possible reason for excellent angiogenesis of BG is that Si ions released from BG can up-regulate the expression of vascular endothelial growth factor, basic fibroblast growth factor and their receptors [33,42]. Secondly, some studies have reported the neovascularization promotion effects of DFO by upregulating the expression of Hif-1α and VEGF. For example, DFO loaded electrospinning scaffolds were proved to promote wound healing in a diabetic rat model. The DFO loaded scaffolds could upregulate the expression of VEGF and Hif-1α of HDF cells and promote tube formation of HUVECs [27]. Similarly, a vascularized 3D printed scaffold was fabricated by immobilizing DFO on a 3D printed scaffold and this scaffold was demonstrated to promote bone regeneration by enhancing vascular ingrowth [43]. In addition to the stimulatory effects of BG and DFO on the angiogenesis of endothelial cells, fast degradation of G-DFO-SA/BG may also benefit the angiogenesis of the wounds as the newly formed blood vessels need room to ingrowth. There would be enough space for cell proliferation and vessels formation after hydrogel degradation [44]. These may be able to explain the better angiogenesis stimulatory effects of G-DFO-SA/BG hydrogel than F-DFO-SA/BG hydrogel.

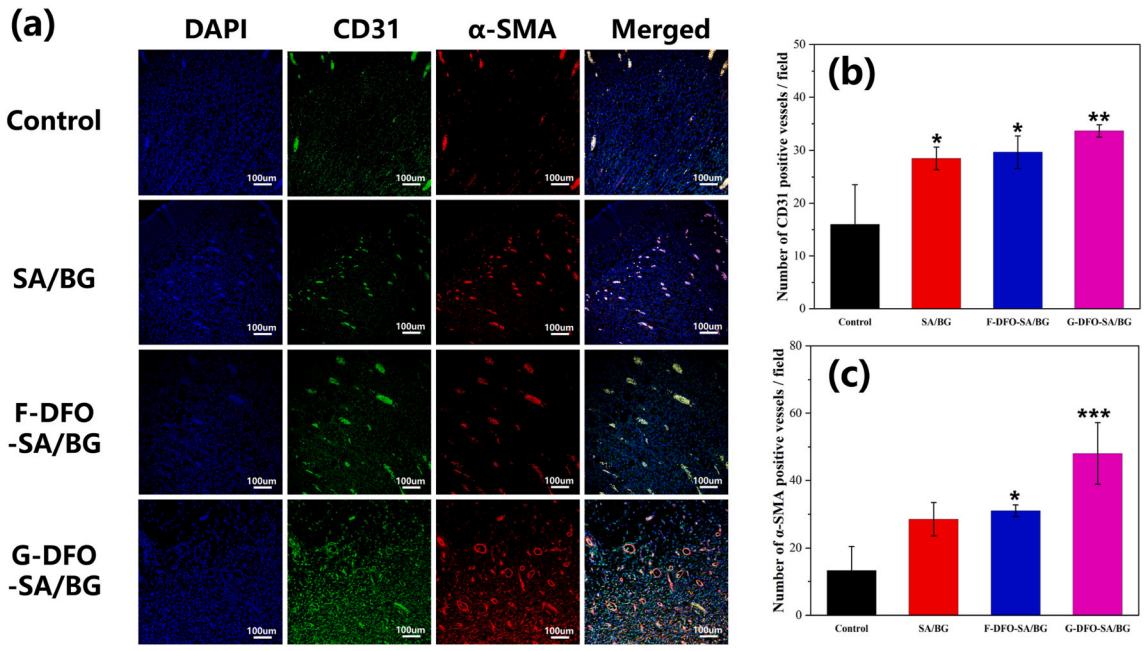

Fig. 7. Vascularization in the wounds treated with nothing (Control) or different hydrogels at day 7. (a) Representative immunofluorescence images of CD31 (green), α-SMA (red) and DAPI (blue) stained tissue samples. (b) Quantitative analysis of CD 31 positive blood vessels in all wounds. (c) Quantitative analysis of α-SMA positive blood vessels in all wounds. All data are compared with Control. * represents $p < 0.05$, ** represents $p < 0.01$ and *** represents $p < 0.001$.

The underlying mechanism of vascularization was confirmed by immunohistochemistry of VEGF and Hif-1α. It can be clearly seen that the wounds treated with F-DFO-SA/BG hydrogel and G-DFO-SA/BG hydrogel had higher expression of VEGF in comparison with the wounds treated with nothing (Fig. 8a). Quantitative analysis showed that VEGF positive area in the wounds treated with F-DFO-SA/BG and G-DFO-SA/BG hydrogels was significantly higher than that in the wounds treated with nothing (Control). Similarly, Hif-1α positive area in wounds treated with F-DFO-SA/BG hydrogel and G-DFO-SA/BG hydrogel was significantly higher than the wounds treated with nothing. Improved

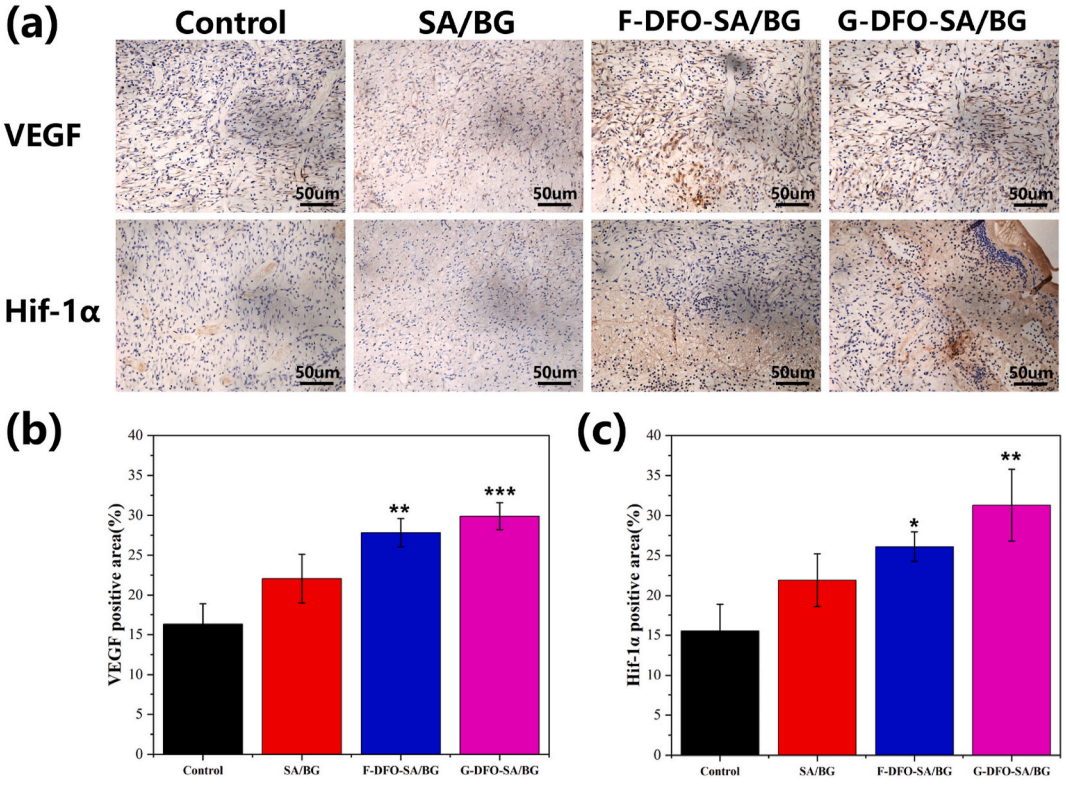

Fig. 8. Immunohistochemistry analysis of VEGF and Hif-1α in wounds at day 7. (a) Represent images of immunohistochemistry staining of VEGF and Hif-1α. Quantitative analysis of VEGF positive area ratio (b) and Hif-1α positive area ratio (c). All data are compared with Control. * represents $p < 0.05$, ** represents $p < 0.01$ and *** represents $p < 0.001$.

expression of VEGF and Hif-1α may be caused by the stimulation of BG and DFO [27,28].

4. Conclusions

In this study, we proposed a new simple strategy for modulating SA hydrogel degradation and promoting tissue infiltration. Degradation modulation of SA was achieved by grafting DFO to SA since grafting of DFO can consume some carboxy groups of SA molecular to reduce the crosslinking density of SA. The designed G-DFO-SA/BG hydrogel showed a faster degradation rate both in vitro and in vivo as compared to SA/BG hydrogel. In addition, G-DFO-SA/BG hydrogel showed strong stimulatory effects on the migration of cells. Thus, when the hydrogels were implanted subcutaneously, G-DFO-SA/BG hydrogel could significantly improve the tissue infiltration as compared with SA/BG hydrogel. Furthermore, both of DFO and BG could stimulate the vascularization of endothelial cells, and they even could work synergistically to promote angiogenesis when the G-DFO-SA/BG hydrogel was applied for skin wound healing. Thus, the G-DFO-SA/BG hydrogel could stimulate angiogenesis and may be able to improve the ingrowth of newly formed blood vessels with its fast degradation, which suggests that G-DFO-SA/BG hydrogel possess a great application potential in tissue regeneration.

Credit author contribution statement

Xin Zhang: Methodology, Formal analysis, Investigation, Writing - original draft, Writing – review. **Ying Li:** Investigation. **Zhijie Ma:** Investigation. **Dan He:** Methodology. **Haiyan Li:** Conceptualization, Validation, Resources, Writing - Reviewing and Editing.

Declaration of competing interest

The authors declare that they have no known competing financial interests or personal relationships that could have appeared to influence the work reported in this paper.

Acknowledgements

This research was supported by the Natural Science Foundation of China (grant No. 31771024 and 31971274) and the Interdisciplinary Program of Shanghai Jiao Tong University (project number: ZH2018ZDA20).

References

[1] A.S. Hoffma, Hydrogels for biomedical applications, Adv. Drug Deliv. Rev. 54 (2002) 3–12, https://doi.org/10.1016/S0169-409X(01)00239-3.
[2] J.L. Drury, D.J. Mooney, Hydrogels for tissue engineering: scaffold design variables and applications, Biomaterials 24 (2003) 4337–4351, https://doi.org/10.1016/s0142-9612(03)00340-5.
[3] C.B. Hutson, J.W. Nichol, H. Aubin, H. Bae, S. Yamanlar, S. Al-Haque, S.T. Koshy, A. Khademhosseini, Synthesis and characterization of tunable poly(ethylene glycol): gelatin methacrylate composite hydrogels, Tissue Eng. A 17 (2011) 1713–1723, https://doi.org/10.1089/ten.TEA.2010.0666.
[4] M. Liu, X. Zeng, C. Ma, H. Yi, Z. Ali, X. Mou, S. Li, Y. Deng, N. He, Injectable hydrogels for cartilage and bone tissue engineering, Bone Res. 5 (2017) 17014, https://doi.org/10.1038/boneres.2017.14.
[5] D.J. McClements, Designing biopolymer microgels to encapsulate, protect and deliver bioactive components: physicochemical aspects, Adv. Colloid Interface Sci. 240 (2017) 31–59, https://doi.org/10.1016/j.cis.2016.12.005.
[6] L.P. da Silva, R.L. Reis, V.M. Correlo, A.P. Marques, Hydrogel-based strategies to advance therapies for chronic skin wounds, Annu. Rev. Biomed. Eng. 21 (2019) 145–169, https://doi.org/10.1146/annurev-bioeng-060418-052422.
[7] T.R. Hoare, D.S. Kohane, Hydrogels in drug delivery: progress and challenges, Polymer 49 (2008) 1993–2007, https://doi.org/10.1016/j.polymer.2008.01.027.
[8] J.A. Hunt, R. Chen, T. van Veen, N. Bryan, Hydrogels for tissue engineering and regenerative medicine, J. Mater. Chem. B 2 (2014) 5319–5338, https://doi.org/10.1039/c4tb00775a.
[9] Y. Tang, S. Lin, S. Yin, F. Jiang, M. Zhou, G. Yang, N. Sun, W. Zhang, X. Jiang, In situ gas foaming based on magnesium particle degradation: a novel approach to fabricate injectable macroporous hydrogels, Biomaterials 232 (2020), https://doi.org/10.1016/j.biomaterials.2019.119727, 119727.
[10] D.R. Griffin, W.M. Weaver, P.O. Scumpia, D. Di Carlo, T. Segura, Accelerated wound healing by injectable microporous gel scaffolds assembled from annealed building blocks, Nat. Mater. 14 (2015) 737–744, https://doi.org/10.1038/nmat4294.
[11] C.E. Brubaker, P.B. Messersmith, Enzymatically degradable mussel-inspired adhesive hydrogel, Biomacromolecules 12 (2011) 4326–4334, https://doi.org/10.1021/bm201261d.
[12] A.C. Daly, L. Riley, T. Segura, J.A. Burdick, Hydrogel microparticles for biomedical applications, Nat. Rev. Mater. 5 (2019) 20–43, https://doi.org/10.1038/s41578-019-0148-6.
[13] M.E. Helgeson, S.C. Chapin, P.S. Doyle, Hydrogel microparticles from lithographic processes: novel materials for fundamental and applied colloid science, Curr. Opin. Colloid Interface Sci. 16 (2011) 106–117, https://doi.org/10.1016/j.cocis.2011.01.005.
[14] K.Y. Lee, D.J. Mooney, Alginate: properties and biomedical applications, Prog. Polym. Sci. 37 (2012) 106–126, https://doi.org/10.1016/j.progpolymsci.2011.06.003.
[15] S. Kargozar, S. Hamzehlou, F. Baino, Can bioactive glasses be useful to accelerate the healing of epithelial tissues? Mater. Sci. Eng. C Mater. Biol. Appl. 97 (2019) 1009–1020, https://doi.org/10.1016/j.msec.2019.01.028.
[16] E. Zeimaran, S. Pourshahrestani, I. Djordjevic, B. Pingguan-Murphy, N.A. Kadri, M. R. Towler, Bioactive glass reinforced elastomer composites for skeletal regeneration: a review, Mater. Sci. Eng. C Mater. Biol. Appl. 53 (2015) 175–188, https://doi.org/10.1016/j.msec.2015.04.035.
[17] Y. Zhu, L. Kong, F. Farhadi, W. Xia, J. Chang, Y. He, H. Li, An injectable continuous stratified structurally and functionally biomimetic construct for enhancing osteochondral regeneration, Biomaterials 192 (2019) 149–158, https://doi.org/10.1016/j.biomaterials.2018.11.017.
[18] M.N. Rahaman, D.E. Day, B.S. Bal, Q. Fu, S.B. Jung, L.F. Bonewald, A.P. Tomsia, Bioactive glass in tissue engineering, Acta Biomater. 7 (2011) 2355–2373, https://doi.org/10.1016/j.actbio.2011.03.016.
[19] S. Kargozar, M. Mozafari, S. Hamzehlou, F. Baino, Using bioactive glasses in the management of burns, Front. Bioeng. Biotechnol. 7 (2019) 62, https://doi.org/10.3389/fbioe.2019.00062.
[20] Q. Zeng, Y. Han, H. Li, J. Chang, Design of a thermosensitive bioglass/agarose-alginate composite hydrogel for chronic wound healing, J. Mater. Chem. B 3 (2015) 8856–8864, https://doi.org/10.1039/c5tb01758k.
[21] Q. Qi, Y. Zhu, G. Liu, Z. Yuan, H. Li, Q. Zhao, Local intramyocardial delivery of bioglass with alginate hydrogels for post-infarct myocardial regeneration, Biomed. Pharmacother. 129 (2020) 110382, https://doi.org/10.1016/j.biopha.2020.110382.
[22] X. Zhang, Y. Zhu, L. Cao, X. Wang, A. Zheng, J. Chang, J. Wu, J. Wen, X. Jiang, H. Li, Z. Zhang, Alginate-aker injectable composite hydrogels promoted irregular bone regeneration through stem cell recruitment and osteogenic differentiation, J. Mater. Chem. B 6 (2018) 1951–1964, https://doi.org/10.1039/c7tb03315j.
[23] K.T. Campbell, R.S. Stilhano, E.A. Silva, Enzymatically degradable alginate hydrogel systems to deliver endothelial progenitor cells for potential revasculature applications, Biomaterials 179 (2018) 109–121, https://doi.org/10.1016/j.biomaterials.2018.06.038.
[24] A. Lueckgen, D.S. Garske, A. Ellinghaus, R.M. Desai, A.G. Stafford, D.J. Mooney, G. N. Duda, A. Cipitria, Hydrolytically-degradable click-crosslinked alginate hydrogels, Biomaterials 181 (2018) 189–198, https://doi.org/10.1016/j.biomaterials.2018.07.031.
[25] A. Lueckgen, D.S. Garske, A. Ellinghaus, D.J. Mooney, G.N. Duda, A. Cipitria, Enzymatically-degradable alginate hydrogels promote cell spreading and in vivo tissue infiltration, Biomaterials 217 (2019), https://doi.org/10.1016/j.biomaterials.2019.119294, 119294.
[26] O. Jeon, S.J. Song, K.-J. Lee, M.H. Park, S.-H. Lee, S.K. Hahn, S. Kim, B.-S. Kim, Mechanical properties and degradation behaviors of hyaluronic acid hydrogels cross-linked at various cross-linking densities, Carbohydr. Polym. 70 (2007) 251–257, https://doi.org/10.1016/j.carbpol.2007.04.002.
[27] H. Chen, P. Jia, H. Kang, H. Zhang, Y. Liu, P. Yang, Y. Yan, G. Zuo, L. Guo, M. Jiang, J. Qi, Y. Liu, W. Cui, H.A. Santos, L. Deng, Upregulating hif-1alpha by hydrogel nanofibrous scaffolds for rapidly recruiting angiogenesis relative cells in diabetic wound, Adv. Healthc. Mater. 5 (2016) 907–918, https://doi.org/10.1002/adhm.201501018.
[28] L. Kong, Z. Wu, H. Zhao, H. Cui, J. Shen, J. Chang, H. Li, Y. He, Bioactive injectable hydrogels containing desferrioxamine and bioglass for diabetic wound healing, ACS Appl. Mater. Interfaces 10 (2018) 30103–30114, https://doi.org/10.1021/acsami.8b09191.
[29] H. Chen, L. Guo, J. Wicks, C. Ling, X. Zhao, Y. Yan, J. Qi, W. Cui, L. Deng, Quickly promoting angiogenesis by using a DFO-loaded photo-crosslinked gelatin hydrogel for diabetic skin regeneration, J. Mater. Chem. B 4 (2016) 3770–3781, https://doi.org/10.1039/c6tb00065g.
[30] Q. Yao, Y. Liu, B. Selvaratnam, R.T. Koodali, H. Sun, Mesoporous silicate nanoparticles/3D nanofibrous scaffold-mediated dual-drug delivery for bone tissue engineering, J. Contr. Release 279 (2018) 69–78, https://doi.org/10.1016/j.jconrel.2018.04.011.
[31] J. Qi, Y. Yan, B. Cheng, L. Deng, Z. Shao, Z. Sun, X. Li, Enzymatic formation of an injectable hydrogel from a glycopeptide as a biomimetic scaffold for vascularization, ACS Appl. Mater. Interfaces 10 (2018) 6180–6189, https://doi.org/10.1021/acsami.7b18535.
[32] M. Tian, X. Chen, Z. Gu, H. Li, L. Ma, X. Qi, H. Tan, C. You, Synthesis and evaluation of oxidation-responsive alginate-deferoxamine conjugates with increased stability and low toxicity, Carbohydr. Polym. 144 (2016) 522–530, https://doi.org/10.1016/j.carbpol.2016.03.014.

[33] H. Yu, J. Peng, Y. Xu, J. Chang, H. Li, Bioglass activated skin tissue engineering constructs for wound healing, ACS Appl. Mater. Interfaces 8 (2016) 703–715, https://doi.org/10.1021/acsami.5b09853.
[34] G. Xu, Y. Xiao, L. Cheng, R. Zhou, H. Xu, Y. Chai, M. Lang, Synthesis and rheological investigation of self-healable deferoxamine grafted alginate hydrogel, J. Polym. Sci. B Polym. Phys. 55 (2017) 856–865, https://doi.org/10.1002/polb.24334.
[35] J. Jang, Y.J. Seol, H.J. Kim, J. Kundu, S.W. Kim, D.W. Cho, Effects of alginate hydrogel cross-linking density on mechanical and biological behaviors for tissue engineering, J. Mech. Behav. Biomed. Mater. 37 (2014) 69–77, https://doi.org/10.1016/j.jmbbm.2014.05.004.
[36] M. Hu, G. Zheng, D. Zhao, W. Yu, Characterization of the structure and diffusion behavior of calcium alginate gel beads, J. Appl. Polym. Sci. 137 (2020), https://doi.org/10.1002/app.48923.
[37] J. Lam, N.F. Truong, T. Segura, Design of cell-matrix interactions in hyaluronic acid hydrogel scaffolds, Acta Biomater. 10 (2014) 1571–1580, https://doi.org/10.1016/j.actbio.2013.07.025.
[38] G. Sun, Y.I. Shen, S. Kusuma, K. Fox-Talbot, C.J. Steenbergen, S. Gerecht, Functional neovascularization of biodegradable dextran hydrogels with multiple angiogenic growth factors, Biomaterials 32 (2011) 95–106, https://doi.org/10.1016/j.biomaterials.2010.08.091.
[39] G. Eke, N. Mangir, N. Hasirci, S. MacNeil, V. Hasirci, Development of a UV crosslinked biodegradable hydrogel containing adipose derived stem cells to promote vascularization for skin wounds and tissue engineering, Biomaterials 129 (2017) 188–198, https://doi.org/10.1016/j.biomaterials.2017.03.021.
[40] Z. Ma, W. Song, Y. He, H. Li, Multilayer injectable hydrogel system sequentially delivers bioactive substances for each wound healing stage, ACS Appl. Mater. Interfaces 12 (2020) 29787–29806, https://doi.org/10.1021/acsami.0c06360.
[41] Y. Zhu, Z. Ma, L. Kong, Y. He, H.F. Chan, H. Li, Modulation of macrophages by bioactive glass/sodium alginate hydrogel is crucial in skin regeneration enhancement, Biomaterials 256 (2020) 120216, https://doi.org/10.1016/j.biomaterials.2020.120216.
[42] H. Li, J. Chang, Bioactive silicate materials stimulate angiogenesis in fibroblast and endothelial cell co-culture system through paracrine effect, Acta Biomater. 9 (2013) 6981–6991, https://doi.org/10.1016/j.actbio.2013.02.014.
[43] Y. Yan, H. Chen, H. Zhang, C. Guo, K. Yang, K. Chen, R. Cheng, N. Qian, N. Sandler, Y.S. Zhang, H. Shen, J. Qi, W. Cui, L. Deng, Vascularized 3D printed scaffolds for promoting bone regeneration, Biomaterials 190-191 (2019) 97–110, https://doi.org/10.1016/j.biomaterials.2018.10.033.
[44] L.H. Han, J.H. Lai, S. Yu, F. Yang, Dynamic tissue engineering scaffolds with stimuli-responsive macroporosity formation, Biomaterials 34 (2013) 4251–4258, https://doi.org/10.1016/j.biomaterials.2013.02.051.